The role of the $P_{11}(1710)$ in the $NN \rightarrow N\Sigma K$ reaction*

A. Sibirtsev¹ †, K. Tsushima² ‡, W. Cassing¹ §, A. W. Thomas² ¶

¹Institut für Theoretische Physik, Universität Giessen

D-35392 Giessen, Germany

²Center for the Subatomic Structure of Matter (CSSM)

and Department of Physics and Mathematical Physics

University of Adelaide, SA 5005, Australia

Abstract

Using the resonance model, which was successfully applied for the study of the $pp \rightarrow p\Lambda K^+$ reaction, we investigate $NN \rightarrow N\Sigma K$ reactions that are expected provide cleaner information about resonance excitations and meson exchange contributions. For this purpose we demonstrate that the invariant mass distribution for the ΣK system, as well as the Dalitz plot for the $NN \rightarrow N\Sigma K$ reaction, provide direct information about the ΣK production mechanism, which can be tested in the near future by experiments at COSY.

PACS: 13.30.-a; 13.75.Ev, 13.75.Cs

Keywords: Decays of baryons; Nucleon-nucleon interactions; Strangeness production; Hyperon-nucleon interactions.

^{*}Supported in part by the Forschungszentrum Jülich and the Australian Research Council

[†]alexandre.sibirtsev@theo.physik.uni-giessen.de

[‡]ktsushim@physics.adelaide.edu.au

 $[\]S$ wolfgang.cassing@theo.physik.uni-giessen.de

[¶]athomas@physics.adelaide.edu.au

1 Introduction

The mechanism of strangeness production in nucleon-nucleon (NN) reactions is still an open problem. In 1960 Ferarri [1] was the first to propose kaon and pion exchanges as a mechanism for strangeness production in NN reactions. It is obvious that one can extend this approach by incorporating other nonstrange mesons, π , η , σ , ρ and ω as well as the known strange mesons, K, K^* and K_1 . In particular, the π , η and ρ mesons are expected to give large contributions because recent experimental data show that they couple strongly to several baryonic resonances (R) which have sizeable decay branches to a hyperon (Y) and a kaon (K). This is especially apparent in the case of $\pi N \to YK$ reactions [2]. Furthermore, among the different meson exchanges the K-meson exchange is of fundamental interest because the kaon-nucleon-hyperon coupling constant, g_{KNY} , is related to the strength for $s\bar{s}$ -pair creation at the KNY vertex. However, as was found in several studies [3, 4, 5, 6], it is not easy to separate the contributions from strange and nonstrange meson exchanges on the basis of the available data. It was shown in Refs. [7, 8, 9] that to reproduce the available experimental data the kaon exchange may not be necessary.

In Ref. [10] we proposed a possibility to distinguish the dominant meson exchanges in the strangeness production, $NN \rightarrow N\Lambda K$, experimentally by reconstructing the invariant mass distribution for the ΛK system. It was found that the strangeness production in the $NN \rightarrow NYK$ reaction could be understood in terms of nonstrange meson exchanges followed by the excitation of an intermediate baryon resonance, R, which decays to a Λ and kaon.

Thus, the YK invariant mass spectrum is a promising way to understand the structure of strangeness production especially with respect to baryonic resonance excitation. Furthermore, we note that at low energies strange meson exchange provides almost the same invariant mass spectrum as an isotropic phase-space distribution for the hyperon-kaon system in the final state. Therefore, there is the possibility to distinguish the kaon exchange contributions from π , η and ρ -meson exchanges, which deviate from isotropic distributions, if they lead to strong baryonic resonance excitations.

Recently, the TOF Collaboration from the COoler SYnchrotron, COSY-Jülich, reported on experimental data for the ΛK invariant mass spectrum [11]. They observe deviations from an isotropic phase space distribution and are close to the predicted spectrum [10]. Obviously, to obtain further insight into the strangeness production mechanism, it is crucial to collect more statistics and also to achieve a better mass resolution for the ΛK system. On the other hand, the observation in Ref. [11] can be considered as a first experimental indication for the excitation of an intermediate baryonic resonance coupled to the ΛK system in the $pp \rightarrow p\Lambda K^+$ reaction.

In this study we calculate the $NN \rightarrow N\Sigma K$ reaction within the same one-meson exchange model used in Refs. [2, 9, 10], which includes π , η and ρ -meson exchanges followed by intermediate state resonance excitations. As is commonly believed, the kaon exchange contribution to Σ production in the NN reaction is almost negligible due to the small $KN\Sigma$ coupling constant (cf. Ref. [12]). Thus we expect the signal

Table 1: The properties of the baryonic resonances included in the model. Confidence levels of the resonances are, $N(1710)^{***}$, $N(1720)^{****}$ and $\Delta(1920)^{***}$ [13].

Resonance (J^P)	Width (MeV)	Decay channel	Branching ratio	Adopted value	
$N(1710)(\frac{1}{2}^+)$	100	$N\pi$	0.10 - 0.20	0.150	
		$N\eta$	0.20 - 0.40	0.300	
		N ho	0.05 - 0.25	0.150	
		ΣK	0.02 - 0.10	0.060	
$N(1720)(\frac{3}{2}^+)$	150	$N\pi$	0.10 - 0.20	0.150	
_		$N\eta$	0.02 - 0.06	0.040	
		N ho	0.70 - 0.85	0.775	
		ΣK	0.02 - 0.05	0.035	
$\Delta(1920)(\frac{3}{2}^+)$	200	$N\pi$	0.05 - 0.20	0.125	
		ΣK	0.01 - 0.03	0.020	

due to resonance excitations in the Σ channel in NN reactions, $R \to \Sigma K$, to be much cleaner than in the Λ production channel. Furthermore, in case of the $pp \to p\Lambda K^+$ reaction there are a few resonances which contribute and therefore smear out the invariant mass distribution for the ΛK system. On the other hand, as will be shown later, the situation for Σ production is much better because the dominant contribution mainly should stem from the N(1710) resonance.

2 The model

The Feynman diagrams relevant for the $NN \rightarrow N\Sigma K$ reaction are shown in Fig. 1. Here R denotes a baryonic resonance which couples to the ΣK channel, while M denotes the exchanged meson $(\pi, \eta \text{ or } \rho)$. The mesons are restricted to those which are observed in the decay channels of the resonances considered.

Since we only take into account those resonances which are experimentally known to decay to a Σ and kaon, and also the branching ratios to the πN , ηN and ρN modes are experimentally measured, all the relevant coupling constants at the MNR and $K\Sigma R$ vertices can be determined from the measured partial widths. The data for the resonances included in the model are summarized in Table 1. Note that some of the data have been modified in Ref. [14]. The $\Delta(1920)$ resonance in the model is treated as an effective resonance which represents the contributions from six individual resonances, i.e. $\Delta(1900)$, $\Delta(1905)$, $\Delta(1910)$, $\Delta(1920)$, $\Delta(1930)$ and $\Delta(1940)$ in line with Ref. [2].

The effective Lagrangian densities relevant for the present study are taken as [2, 9, 10]

$$\mathcal{L}_{\pi NN} = -ig_{\pi NN} \bar{N} \gamma_5 \vec{\tau} N \cdot \vec{\pi}, \tag{1}$$

$$\mathcal{L}_{\eta NN} = -ig_{\eta NN}\bar{N}\gamma_5 N\eta, \qquad (2)$$

$$\mathcal{L}_{\rho NN} = -g_{\rho NN} \left(\bar{N} \gamma^{\mu} \vec{\tau} N \cdot \vec{\rho}_{\mu} + \frac{\kappa}{2m_{N}} \bar{N} \sigma^{\mu\nu} \vec{\tau} N \cdot \partial_{\mu} \vec{\rho}_{\nu} \right), \tag{3}$$

$$\mathcal{L}_{\pi NN(1710)} = -ig_{\pi NN(1710)} \left(\bar{N}(1710) \gamma_5 \vec{\tau} N \cdot \vec{\pi} + \bar{N} \gamma_5 \vec{\tau} N(1710) \cdot \vec{\pi} \right), \tag{4}$$

$$\mathcal{L}_{\eta NN(1710)} = -ig_{\eta NN(1710)} \left(\bar{N}(1710) \gamma_5 N \eta + \bar{N} \gamma_5 N(1710) \eta \right), \tag{5}$$

$$\mathcal{L}_{\rho NN(1710)} = -g_{\rho NN(1710)} \left(\bar{N}(1710) \gamma^{\mu} \vec{\tau} N \cdot \vec{\rho}_{\mu} + \bar{N} \gamma^{\mu} \vec{\tau} N(1710) \cdot \vec{\rho}_{\mu} \right), \qquad (6)$$

$$\mathcal{L}_{\pi NN(1720)} = \frac{g_{\pi NN(1720)}}{m_{\pi}} \left(\bar{N}^{\mu} (1720) \vec{\tau} N \cdot \partial_{\mu} \vec{\pi} + \bar{N} \vec{\tau} N^{\mu} (1720) \cdot \partial_{\mu} \vec{\pi} \right), \tag{7}$$

$$\mathcal{L}_{\eta NN(1720)} = \frac{g_{\eta NN(1720)}}{m_{\eta}} \left(\bar{N}^{\mu} (1720) N \partial_{\mu} \eta + \bar{N} N^{\mu} (1720) \partial_{\mu} \eta \right), \tag{8}$$

$$\mathcal{L}_{\rho NN(1720)} = -ig_{\rho NN(1720)} \left(\bar{N}^{\mu} (1720) \gamma_5 \vec{\tau} N \cdot \vec{\rho}_{\mu} + \bar{N} \gamma_5 \vec{\tau} N^{\mu} (1720) \cdot \vec{\rho}_{\mu} \right), \quad (9)$$

$$\mathcal{L}_{\pi N \Delta(1920)} = \frac{g_{\pi N \Delta(1920)}}{m_{\pi}} \left(\bar{\Delta}^{\mu} (1920) \overrightarrow{\mathcal{I}} N \cdot \partial_{\mu} \vec{\pi} + \bar{N} \overrightarrow{\mathcal{I}}^{\dagger} \Delta^{\mu} (1920) \cdot \partial_{\mu} \vec{\pi} \right), \quad (10)$$

$$\mathcal{L}_{K\Sigma N(1710)} = -ig_{K\Sigma N(1710)} \left(\bar{N}(1710) \gamma_5 \vec{\tau} K \cdot \overrightarrow{\Sigma} + \overrightarrow{\overline{\Sigma}} \cdot \bar{K} \vec{\tau} \gamma_5 N(1710) \right), \quad (11)$$

$$\mathcal{L}_{K\Sigma N(1720)} = \frac{g_{K\Sigma N(1720)}}{m_K} \left(\bar{N}^{\mu}(1720) \vec{\tau}(\partial_{\mu}K) \cdot \overrightarrow{\Sigma} + \overrightarrow{\overline{\Sigma}} \cdot (\partial_{\mu}\bar{K}) \vec{\tau} N^{\mu}(1720) \right), (12)$$

$$\mathcal{L}_{K\Sigma\Delta(1920)} = \frac{g_{K\Sigma\Delta(1920)}}{m_K} \left(\overline{\Delta}^{\mu}(1920) \overrightarrow{\mathcal{I}} \cdot \overrightarrow{\Sigma} \partial_{\mu} K + (\partial_{\mu} \overline{K}) \overrightarrow{\overline{\Sigma}} \cdot \overrightarrow{\mathcal{I}}^{\dagger} \Delta^{\mu}(1920) \right) (13)$$

where the ratio of the tensor to the vector coupling constant at the ρNN vertex in Eq. (3) is used as $\kappa = f_{\rho NN}/g_{\rho NN} = 6.1$ [15]. The operators $\overrightarrow{\mathcal{I}}$ and $\overrightarrow{\mathcal{K}}$ are defined by

$$\overrightarrow{\mathcal{I}}_{M\mu} \equiv \sum_{\ell=\pm 1,0} (1\ell \frac{1}{2}\mu | \frac{3}{2}M) \hat{e}_{\ell}^*, \tag{14}$$

$$\overrightarrow{\mathcal{K}}_{MM'} \equiv \sum_{\ell=\pm 1,0} (1\ell^{\frac{3}{2}}M'|\frac{3}{2}M)\hat{e}_{\ell}^*, \tag{15}$$

where M, μ and M' denote the third components of the isospin projections, respectively, while $\vec{\tau}$ are the Pauli matrices. N, N(1710), N(1720) and $\Delta(1920)$ stand for the nucleon fields and the baryon resonances, respectively; they are expressed by $\bar{N} = (\bar{p}, \bar{n})$ and $\bar{\Delta}(1920) = (\bar{\Delta}(1920)^{++}, \bar{\Delta}(1920)^{+}, \bar{\Delta}(1920)^{0}, \bar{\Delta}(1920)^{-})$ in isospin space. The physical representations of the fields are given by: $K^{T} = (K^{+}, K^{0}), \bar{K} = (K^{-}, \bar{K}^{0}), \pi^{\pm} = (\pi_{1} \mp i\pi_{2})/\sqrt{2}, \pi^{0} = \pi_{3}$ and similarly for the ρ -meson fields, and $\Sigma^{\pm} = (\Sigma_{1} \mp i\Sigma_{2})/\sqrt{2}, \Sigma^{0} = \Sigma_{3}$, respectively, where the superscript T means the transposition operation. (Notice the similarity of $\vec{\tau} \cdot \vec{\pi}$ and $\vec{\tau} \cdot \vec{\Sigma}$.) The meson fields are defined as either annihilating or creating the physical particle or anti-particle states, respectively.

For the propagators, $iS_F(p)$ for spin 1/2 and $iG^{\mu\nu}(p)$ for spin 3/2 resonances, we use:

$$iS_F(p) = i \frac{\gamma \cdot p + m}{p^2 - m^2 + im\Gamma^{full}}, \qquad (16)$$

Table 2:	Coupling	constants	and	cut-off	parameters	used	in	the	present	study.

vertex	$g^2/4\pi$	cut-off (MeV)
πNN	14.4	1050
$\pi NN(1710)$	2.05×10^{-1}	800
$\pi NN(1720)$	4.13×10^{-3}	800
$\pi N\Delta(1920)$	1.13×10^{-1}	500
ηNN	5.00	2000
$\eta NN(1710)$	2.31	800
$\eta NN(1720)$	1.03×10^{-1}	800
ρNN	0.74	920
$\rho NN(1710)$	$3.61 \times 10^{+1}$	800
$\rho NN(1720)$	$1.43 \times 10^{+2}$	800
$K\Sigma N(1710)$	4.66	800
$K\Sigma N(1720)$	2.99×10^{-1}	800
$K\Sigma\Delta(1920)$	3.08×10^{-1}	500

$$iG^{\mu\nu}(p) = i\frac{-P^{\mu\nu}(p)}{p^2 - m^2 + im\Gamma^{full}},$$
 (17)

with

$$P^{\mu\nu}(p) = -(\gamma \cdot p + m) \left[g^{\mu\nu} - \frac{1}{3} \gamma^{\mu} \gamma^{\nu} - \frac{1}{3m} (\gamma^{\mu} p^{\nu} - \gamma^{\nu} p^{\mu}) - \frac{2}{3m^2} p^{\mu} p^{\nu} \right], \tag{18}$$

where m and Γ^{full} stand for the mass and full decay width of the corresponding resonances.

To account for the nonlocality or finite size of hadrons we introduce form factors, $F_M(\vec{q})$, at the relevant interaction vertices,

$$F_M(\vec{q}) = \left(\frac{\Lambda_M^2}{\Lambda_M^2 + \vec{q}^2}\right)^n,\tag{19}$$

with \vec{q} denoting the momentum of the exchanged meson and n=1 for the π and η -mesons and n=2 for the ρ -meson, respectively, while Λ_M denotes the cut-off parameter. For the calculation of the $NN \to N\Sigma K$ reactions we adopt the same form factors, coupling constants and cut-off parameters which were used in Refs. [2, 9, 12]. It should be emphasized that the coupling constants and form factors necessary for the calculation of the $NN \to N\Sigma K$ reactions have been already fixed to reproduce the $\pi N \to YN$ and $pp \to N\Lambda K$ total cross section data. The coupling constants and cut-off parameters used in the calculation are summarized in Table 2.

3 Analysis of model uncertainties

In this section we analyze the contributions from different meson exchanges and the sensitivity to the model parameters.

From a first look at the coupling constants listed in Table 2 one expects that the dominant contribution for the $NN \rightarrow N\Sigma K$ reaction should come from the N(1710) or P_{11} resonance. The $g_{K\Sigma N(1710)}$ coupling constant is one order of magnitude larger than $g_{K\Sigma N(1720)}$ and $g_{K\Sigma\Delta(1920)}$. Although the $g_{\rho NN(1720)}$ coupling constant is larger than $g_{\rho NN(1710)}$, it is compensated by the small value for $g_{K\Sigma N(1720)}$ coupling constant. The actual calculated results support this simple estimate.

In Fig. 2 we show the decomposition of the contributions from each resonance to the energy dependence of the $pp \rightarrow p\Sigma^0 K^+$ total cross section, plotted as a function of the excess energy $\epsilon = \sqrt{s} - m_N - m_{\Sigma} - m_K$. The calculations were performed without including the ΣN final state interaction (FSI), which is expected to be important at energies very close to threshold [16, 17]. Indeed, the results shown in Fig. 2 confirm the expectation that the dominant contribution comes from the P_{11} resonance. In addition, the contribution from the P_{33} baryonic resonance is almost negligible.

Next, we analyze the contributions from the different meson exchanges. It is not straightforward to estimate, which meson exchange gives a dominant contribution to the ΣK production in nucleon-nucleon collisions by just looking at the data in Table 2. We, therefore, show in Fig. 3 the separate contributions from π , η and ρ -meson exchanges to the energy dependence of the $pp \rightarrow p\Sigma^0 K^+$ and $pp \rightarrow p\Sigma^+ K^0$ total cross sections. We find that the contributions from π and η exchange are important at low energies, while the ρ -meson exchange contribution dominates at excess energies ϵ above 1 GeV.

A crucial question is the sensitivity of the results to the coupling constants and cut-off parameters which cannot be fixed solely from the experimental data within the model. The situation for the π -meson exchange is rather clear; the coupling constant and the form factor at the πNN vertex are well under control from the study of NN interactions. In addition, according to the investigations of the $\pi N \to \Sigma K$ reactions [2], the πNR and $K\Sigma R$ vertices are fixed consistently by the existing experimental data. Fig. 4 shows a comparison between the model calculations and the data on $\pi N \to \Sigma K$ cross sections. With the set of the parameters listed in Tab. 1 the model reasonably reproduces the different reaction channels: $\pi^+ p \to K^+ \Sigma^+$, $\pi^- p \to K^0 \Sigma^0$, $\pi^+ n \to K^+ \Sigma^0$ and $\pi^- p \to K^+ \Sigma^-$.

On the other hand, the situation for the η -meson exchange is less obvious. Since the contribution from η -exchange is important at low energies (cf. Fig. 3), we have to discuss the status of the ηNN coupling constant in more detail.

As reviewed by Tiator, Benhold and Kamalov [18], the ηNN coupling constant has still large uncertainties. The values for $g_{\eta NN}$ vary between 1 and 9 and depend substantially on the model applied to describe the data. Furthermore, the experimental data themselves have large uncertainties and do not allow to extract a precise value for $g_{\eta NN}$. When using the one-boson exchange potential to fit the nucleon-nucleon phase shifts [19] one requires $6 \le g_{\eta NN} \le 9$. However, the analysis itself is not sensitive enough to the η -meson exchange. On the other hand, the $\pi^- p \to \eta n$ data restrict the value to be small, $g_{\eta NN} = 2.7 \div 4.6$ [18].

Furthermore, a fit to the total cross section for the $\gamma p \rightarrow \eta p$ reaction requires $g_{\eta NN}=1.1$ in the case of pseudoscalar coupling and $f_{\eta NN}=8.7$ for pseudovector coupling [18]. Thus the total cross section is not sensitive enough to evaluate the

coupling constant. However, the authors of Ref. [18] suggest a value, $g_{\eta NN}$ =2.24, which is extracted from the description of the angular distribution. A global analysis of both meson scattering and photon induced reactions on the nucleon, performed recently by Feuster and Mosel [20], yields a value $g_{\eta NN}$ =1.0.

Based on SU(3) symmetry the $g_{\eta NN}$ coupling constant is related to the $g_{\pi NN}$ as [21]

$$g_{\eta NN} = \frac{-\alpha + 3(1-\alpha)}{\sqrt{3}} g_{\pi NN}$$
 (20)

with α =0.6 when combined with the SU(6) quark model; this value for α gives $g_{\eta NN} \simeq 4.65$.

In our calculation we use the value $g_{\eta NN}$ =7.9 taken from the Bonn NN potential model [15]. Considering the uncertainty discussed above for the ηNN coupling constant, we have investigated how the calculated results are affected by varying the value for $g_{\eta NN}$. The deviations due to the different values for $g_{\eta NN}$ for the contribution from the η -exchange (shown in Fig. 3 for $g_{\eta NN}$ =7.9) then vary by factors of 1/60 to 1.3, respectively.

In addition, there are also uncertainties in the resonance properties. The latest issue of the Review of Particle Data [14] no longer lists the branching ratios for the $N(1710) \rightarrow \eta N$ and $N(1710) \rightarrow \rho N$ channels. Thus, the coupling constants $g_{\eta NN(1710)}$ and $g_{\rho NN(1710)}$ also involve uncertainties on the present experimental confidence level. A similar situation also holds for the N(1720) resonance. Note, however, that the ρ couplings have been already fixed by our previous study on Λ -hyperon production in NN collisions [9].

4 Comparison with data

The data for $NN \rightarrow N\Sigma K$ reactions are available at excess energies larger than 300 MeV. In Fig. 5 we show the calculated energy dependence of the total cross sections for the $pp \rightarrow p\Sigma^+ K^0$, $pp \rightarrow p\Sigma^0 K^+$ and $pp \rightarrow n\Sigma^+ K^+$ reactions (solid lines) in comparison with the experimental data (dots) from Ref. [22]. Our model reproduces all these reaction channels reasonably well with the same set of parameters.

However, the situation is different for the $np\to p\Sigma^0 K^0$ and $np\to p\Sigma^- K^+$ reactions. The energy dependence of the total cross sections for these reactions is shown in Fig. 6; here our calculations (solid lines) substantially overestimate the experimental data (full dots) from Ref. [22]. As illustrated in Fig. 3, at excess energies above 1 GeV the dominant contribution stems from ρ -meson exchange according to our model. This phenomenon is shown in Fig. 7, where the meson exchange contributions are displayed separately. This implies that almost all available data for the $NN\to N\Sigma K$ reaction are dominantly governed by the parameters for ρ -exchange, while the model parameters, together with those for ρ -exchange, have been fixed to reproduce optimally the existing total cross section data for the $pp\to p\Lambda K^+$ and $pp\to N\Sigma K$ reactions at excess energies around 1 GeV. Thus the data for the $np\to p\Sigma K$ reaction at excess energies larger than 1 GeV clearly indicate the limitations of our model.

Nevertheless, we may check the consistency of the data. For this purpose we show the ratios of the total cross sections for the $np\to p\Sigma^-K^+$ to $pp\to p\Sigma^+K^0$ both for the experimental data (full dots with error bars) and the calculated results (solid line) in Fig. 8. In a simple one-boson exchange picture (tree-level), only neutral mesons can be exchanged in the $pp\to p\Sigma^+K^0$ reaction, while both neutral and charged mesons can be exchanged in the $np\to p\Sigma^-K^+$ reaction. Furthermore, the isospin factor for charged meson exchange at the meson-nucleon-nucleon vertex is a factor of $\sqrt{2}$ larger than that for the neutral meson. If we neglect the small contribution from η exchange as in Fig. 7, our explicit calculation shows that the direct amplitudes for π and ρ exchange followed by N(1710) and N(1720) resonance excitation, give a factor of two larger contributions to the $np\to p\Sigma^-K^+$ reaction relative to those for the $pp\to p\Sigma^+K^0$ reaction. Thus, we may naively expect that the total cross section for the $np\to p\Sigma^-K^+$ reaction should be larger than that for $pp\to p\Sigma^+K^0$.

However, the ratios for the experimental data in Fig. 8 (the dots) clearly contradict this expectation; the ratios become even smaller than one. The calculated results (solid line) reasonably agree with the simple estimate made above. We note that the available data for the ΣK production in np collisions collected in Ref. [22] were obtained by the group of Ansorge et al. [23] alone. The data were taken with a neutron beam and the CERN 2 m hydrogen bubble chamber; the systematic uncertainty due to the beam normalization $\simeq 13\%$ is not shown in our figures. Thus, we would like to urge experimental collegues to collect more data for the $np \rightarrow N\Sigma K$ reaction in order to resolve this systematic discrepancy.

Finally, in Fig. 9 we show the $pp \rightarrow p\Sigma^0 K^+$ total cross section for a larger scale of excess energies, as relevant for COSY, such that one can examine the effect of final state interactions in more detail. Note, that our calculations were performed without the inclusion of FSI. Thus we expect that the present results should deviate from the experimental data at small excess energies. Deviations of our calculation [9] from the data [24, 25] at excess energies $\epsilon \leq 10$ MeV have been also noticed for the $pp \rightarrow p\Lambda K^+$ reaction. It was argued both experimentally [16] and theoretically [17], that at energies very close to the reaction threshold the production mechanism is strongly distorted by the final state interaction between the hyperon and the nucleon.

One of the common ways [26, 27, 28, 29] to account for FSI is using the Watson-Migdal theorem [30, 31], which expresses the total reaction amplitude as a product of the production amplitude and the on mass-shell $YN \rightarrow YN$ scattering amplitude. However, this approach was recently criticized by Hanhart and Nakayama [32] focusing on the on-shell treatment and factorization of the reaction amplitude. It was also suggested by Meißner [33] that the treatment of FSI might be too simplistic in the Watson-Migdal scheme.

In addition, we note that the knowledge of the YN scattering amplitudes is still unsatisfactory. Although there have been extensive theoretical studies of the hyperon-nucleon interaction [34, 35, 36, 37, 38, 39], the YN interaction models from Nijmegen [36] and Jülich [37] predict completely different results for the $pn \rightarrow \Lambda p$ reaction as recently shown by Parreno et al. [40]. This implies that the introduction of FSI corrections in the calculation is strongly model dependent even within the on mass-shell Watson-Migdal approximation. The situation is even more compli-

cated [3] because the $\Sigma N \leftrightarrow \Lambda N$ channel coupling becomes stronger at energies close to the threshold. It is therefore not so easy to improve the $NN \to NYK$ calculations near threshold by taking into account FSI corrections in an unambiguous manner, as compared to the treatment proposed in Ref. [17]. As a consequence, we discard the explicit calculation of FSI corrections and rather concentrate our study on excess energies larger than 40 MeV, where FSI and the $\Sigma N \leftrightarrow \Lambda N$ channel coupling are expected to be small.

5 Analysis of the reaction dynamics within the model

To obtain insight into the dynamics of hyperon production in NN collisions we demonstrated in Ref. [12] that the invariant mass spectrum for the ΛK system indeed provides a clue to the Λ production mechanism. The situation also holds true for the $NN \rightarrow N\Sigma K$ reaction. If the $NN \rightarrow N\Sigma K$ reaction proceeds through the excitation of baryonic resonances one might observe a characteristic distribution for the ΣK invariant mass, which reflects the excitation of the intermediate baryonic resonance. As shown in Ref. [10] the invariant mass distribution for the hyperon-nucleon system extends to the upper limit of $m_Y + m_K + \epsilon$ and, thus, depends on the excess energy ϵ . Since the typical widths of the baryonic resonances (cf. Table 1) range from 100 to 200 MeV, the distribution may be affected by intermediate baryonic resonance excitations for $\epsilon > 100$ MeV (half width of 200 MeV). This also implies that the invariant mass spectrum at energies near the reaction threshold, i.e., small excess energies, will not show a clear signal of the baryonic resonance excitation. Since the invariant mass distribution ranges from the threshold energy to the threshold energy plus excess energy, the shape of the invariant mass distribution cannot be affected noticeably if the excess energy is smaller than the resonance width.

In Fig. 10 we show the ΣK invariant mass distribution for the $pp \rightarrow p\Sigma^0 K^+$ reaction calculated at an excess energy of 100 MeV. The dashed histogram is the sum of the contributions from the N(1720) and $\Delta(1920)$ resonances, while the solid histogram corresponds to the total sum of contributions from the N(1710), N(1720) and $\Delta(1920)$ resonances. It is clear that the dominant contribution comes from the N(1710). For comparison, we also show the phase space distribution normalized to the same total cross section (solid line). At this excess energy the deviation from the phase-space distribution due to resonance excitations is already noticeable.

In Fig. 11 we show again the ΣK invariant mass distribution for the $pp \rightarrow p\Sigma^0 K^+$ reaction, but at an excess energy ϵ =200 MeV. The solid histogram is the sum of the contributions from all the resonances, N(1710), N(1720) and $\Delta(1920)$, while the solid line is the phase-space distribution normalized to the same total cross section. At this excess energy the deviation from the phase-space distribution becomes more pronounced and the signal from the N(1710) excitation can be detected at the peak position of the ΣK invariant mass, $M_{\Sigma K} \simeq 1.76$ GeV. Recall, that the contributions from the other resonances are small.

As was proposed by the COSY-11 [16] and TOF- [11] Collaborations a more

precise analysis can be performed in terms of a Dalitz plot to understand the ΣK production mechanism. In Fig. 12 we show the Dalitz plot calculated for the $pp \rightarrow p\Sigma^0 K^+$ reaction at the excess energy $\epsilon = 100$ MeV; i.e. the ΣN invariant mass versus the ΣK invariant mass. In Fig. 12 the larger squares denote a higher density of the invariant mass distribution. In case of strong final state interactions between the Σ and nucleon one would expect an enhancement in the lower region of the ΣN invariant mass. According to the hyperon-nucleon potential models of the Nijmegen [36, 39] and Jülich [37, 38] groups the hyperon-nucleon interaction becomes very strong at the ΣN invariant mass below $\simeq 2.17$ GeV. Thus, FSI can substantially distort the N(1710) signal. Indeed, Fig. 12 illustrates that there is a structure around $M_{\Sigma K}=1.75$ GeV, but this is due to the contribution from the N(1710) resonance which overlaps with the $M_{\Sigma N}$ region, where the influence of FSI might be substantial (cf. Fig. 10).

In Fig. 13 we show the Dalitz plot for the $pp \rightarrow p\Sigma^0 K^+$ reaction at an excess energy ϵ =200 MeV. The situation is much clearer than in the case ϵ = 100 MeV, shown in Fig. 12, since the structure due to the N(1710) resonance is well separated from the lower range of ΣN invariant mass. Thus, we expect that the Dalitz plots for the $M_{\Sigma K}$ and $M_{\Sigma N}$ invariant masses should be a very useful tool for understanding the dynamics of the $NN \rightarrow N\Sigma K$ reaction.

6 Summary

Within a simple model of one-boson exchange followed by baryonic resonance excitation we have investigated the $NN \rightarrow N\Sigma K$ reactions. Our model includes only those mesons which are observed to couple to the baryonic resonances which themselves are known to decay to a Σ -hyperon and K-meson. Thus only the nonstrange meson exchanges $(\pi, \eta \text{ and } \rho)$ were taken into account.

We demonstrated that our model could reproduce reasonably well the available total cross section data for the $pp{\to}N\Sigma K$ reaction, while it overestimated systematically the data for the channel $np{\to}N\Sigma K$ at higher energy. Concerning the experimental data for the $np{\to}N\Sigma K$ reaction, we investigated the data consistency in terms of a simple isospin model using the one-boson exchange picture. We demonstrated, that it is essential to have new experimental data on neutron induced Σ production.

We also showed that the ΣK invariant mass spectrum provides a powerful method to understand the $NN \rightarrow N\Sigma K$ reaction mechanism. In the present approach the dominant contribution to $NN \rightarrow N\Sigma K$ reactions comes from the N(1710) resonance and it substantially affects the ΣK invariant mass distribution. Our results suggest that the signal due to the N(1710) resonance excitation can be detected experimentally at excess energies around 100 MeV.

Finally, we analyzed the Dalitz plot based on our calculations and presented the distribution of the ΣN invariant mass versus the ΣK invariant mass. This analysis shows a characteristic structure due to the N(1710) resonance that can be well distinguished from the lower region in the ΣN invariant mass, where the final state interaction between the Σ and nucleon might be strong. However, a much cleaner

signal of the N(1710) resonance excitation can be detected at excess energies larger than 100 MeV, e.g. at 200 MeV.

References

- [1] E. Ferrari, Phys. Rev. 120 (1960) 988; Nuovo Cim. 15 (1960) 652.
- [2] K. Tsushima, S.W. Huang and Amand Faessler, Phys. Lett. B 337 (1994) 245;
 J. Phys. G21 (1995) 33; Australian. J. Phys. 50 (1997) 35.
- [3] J.M. Laget, Phys. Lett. B 259 (1991) 24.
- [4] A. Deloff, Nucl. Phys. A 505 (1989) 583.
- [5] G.Q. Li and C.M. Ko, Nucl. Phys. A594 (1995) 439.
- [6] A. Sibirtsev, Phys. Lett. B 359 (1995) 29.
- [7] T. Yao, Phys. Rev. 125 (1962) 1048.
- [8] J.Q. Wu and C.M. Ko, Nucl. Phys. A 499 (1989) 810.
- K. Tsushima, A. Sibirtsev, A. W. Thomas, Phys. Lett. B 390 (1997) 29;
 K. Tsushima, A. Sibirtsev, A. W. Thomas, G.Q. Li, nucl-th/9801063, to appear in Phys. Rev. C 59 (1999).
- [10] A. Sibirtsev, K. Tsushima and A.W. Thomas, Phys. Lett. B 421 (1998) 59.
- [11] R. Bilger et al., Phys. Lett. B429 (1998) 195.
- [12] A. Sibirtsev and W. Cassing, Preprint INP-1787/PH, Krakow; nucl-th/9802019.
- [13] Particle Data Group, Phys. Rev. D 50 (1994).
- [14] Particle Data Group, Eur. J. Phys. A 3 (1998).
- [15] R. Machleidt, Adv. Nucl. Phys. 19 (1989) 189.
- [16] J.T. Balewski et al., Eur. Phys. J. A 2 (1998) 99.
- [17] A. Sibirtsev and W. Cassing, nucl-th/9802025.
- [18] L. Tiator, C. Benhold and S.S. Kamalov, Nucl. Phys. A 580 (1994) 455.
- [19] R. Brockmann and R. Machleidt, Phys. Rev. C 42 (1990) 1965.
- [20] T. Feuster and U. Mosel, nucl-th/9803057.
- [21] P.A. Carruthers, Introduction to Unitary Symmetry, 1966, John Wiley & Sons.
- [22] Landolt-Börnstein, New Series, ed. H. Schopper, I/12 (1988).

- [23] R.E. Ansorge et al. Nucl. Phys. B 103 (1976) 509.
- [24] J.T. Balewski et al, Phys. Lett. B 420 (1998) 211.
- [25] J.T. Balewski et al., Nucl. Phys. A 629 (1998) 164c.
- [26] A. Sibirtsev and W. Cassing, Eur. Phys. J. A 2 (1998) 333.
- [27] R. Shyam and U. Mosel, Phys. Lett. B 426 (1998) 1.
- [28] A. Moalem et al., Nucl. Phys. A 589 (1995) 649.
- [29] V. Bernard, N. Kaiser, Ulf-G. Meißner, nucl-th/9806013.
- [30] K.M. Watson, Phys. Rev. 88 (1952) 1163.
- [31] A.B. Migdal, JETP 1 (1955) 2.
- [32] C. Hanhard and K. Nakayama, nucl-th/9809059
- [33] Ulf-G. Meißner, nucl-th/9810015.
- [34] M.M. Nagels, Th.A. Rijken and J.J. de Swart, Phys. Rev. D 20 (1979) 1633.
- [35] Y. Takahashi et al., Nucl. Phys. A 336 (1980) 347.
- [36] P.M.M. Maessen, Th.A. Rijken and J.J. de Swart, Phys. Rev. C 40 (1989) 2226.
- [37] B. Holzenkamp, K. Holinde and J. Speth, Nucl. Phys. A 500 (1989) 485.
- [38] A. Reuber, K. Holinde and J. Speth, Nucl. Phys. A 570 (1994) 543.
- [39] Th.A. Rijken, V.G.J. Stoks and Y. Yamamoto, nucl-th/9807082.
- [40] A. Parreno et al., nucl-th/9809053.

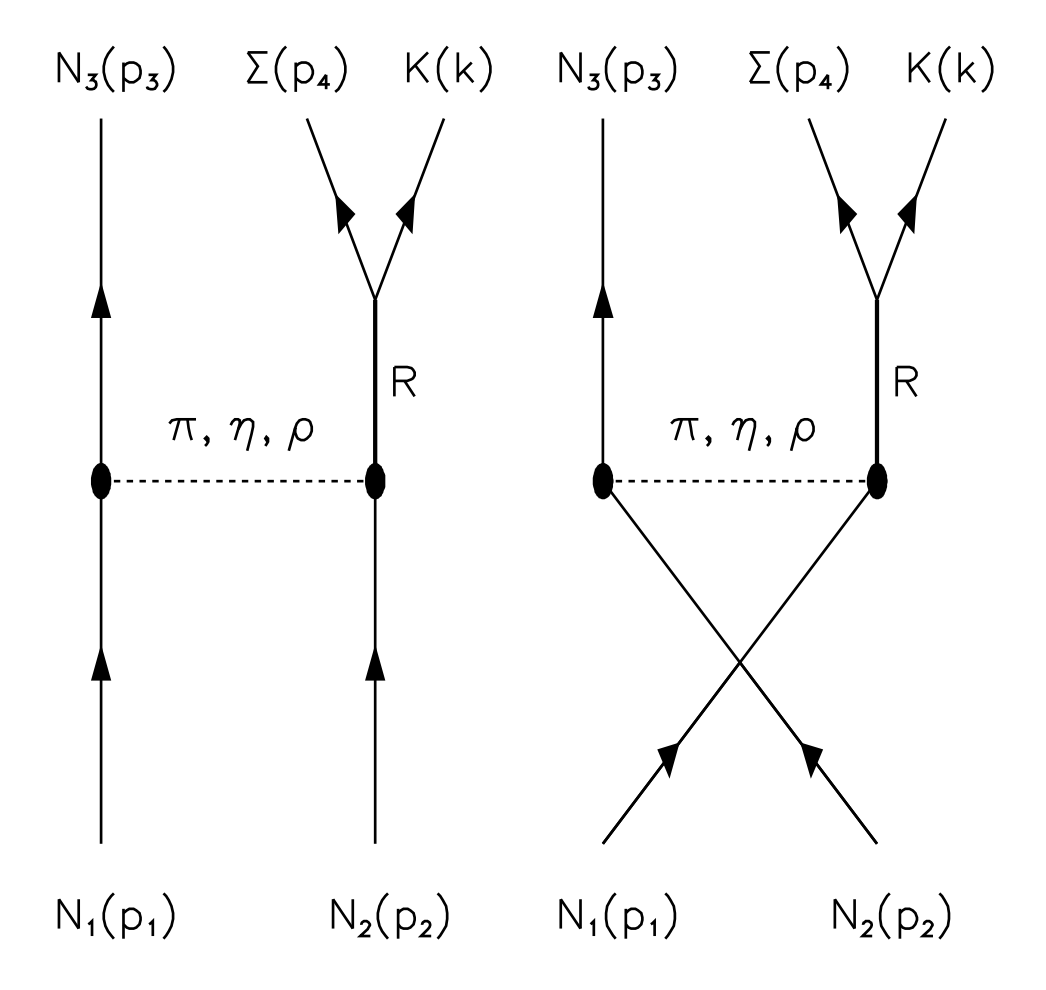


Figure 1: Feynman diagrams for the reaction $NN \rightarrow N\Sigma K$ considered in the model.

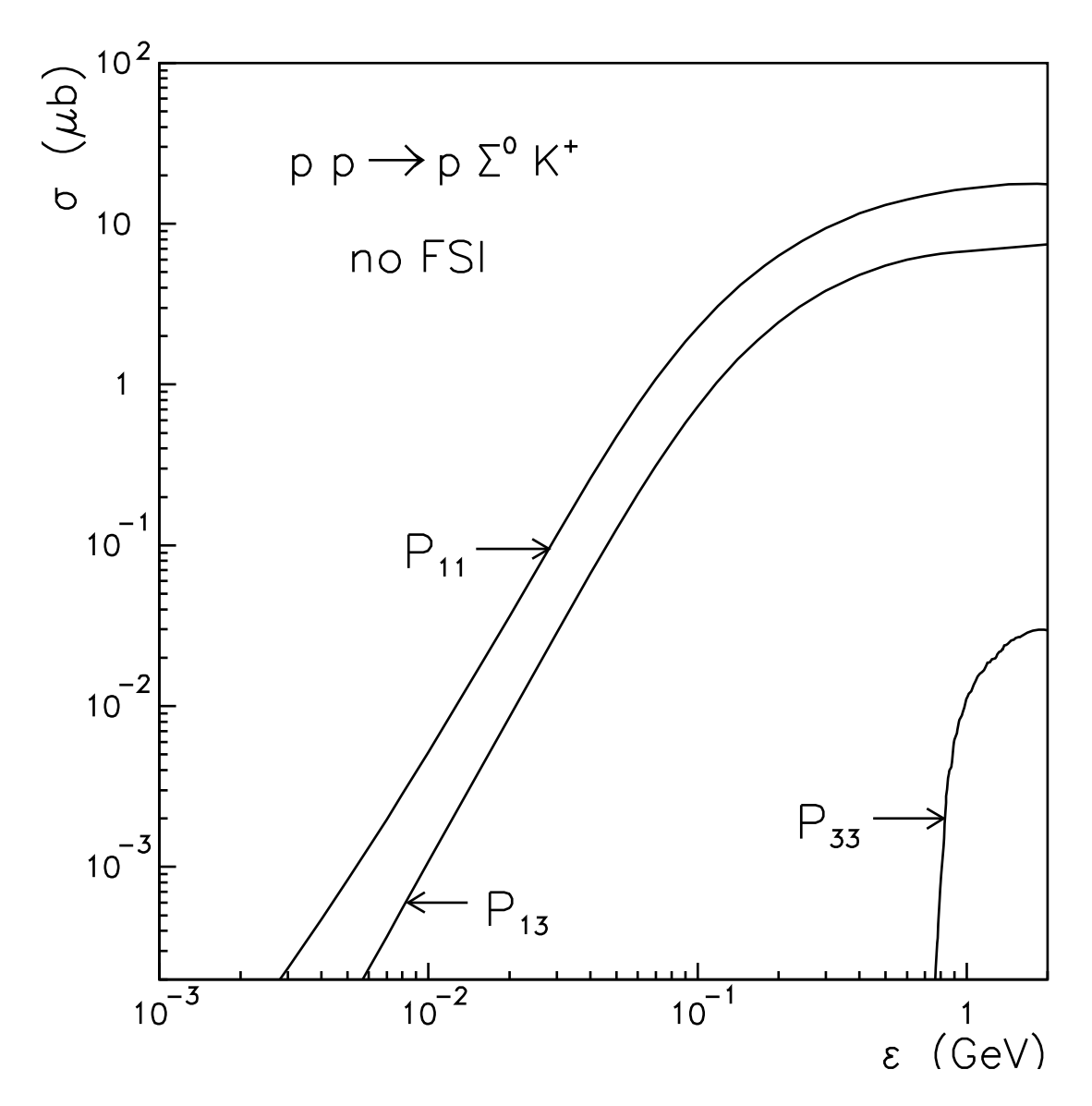


Figure 2: Decomposition of the total cross section in terms of individual resonance contributions, N(1710) (P_{11}) , N(1720) (P_{13}) and $\Delta(1920)$ (P_{33}) resonances for the $pp \rightarrow p\Sigma^0 K^+$ reaction. The calculation was performed without the inclusion of final state interactions.

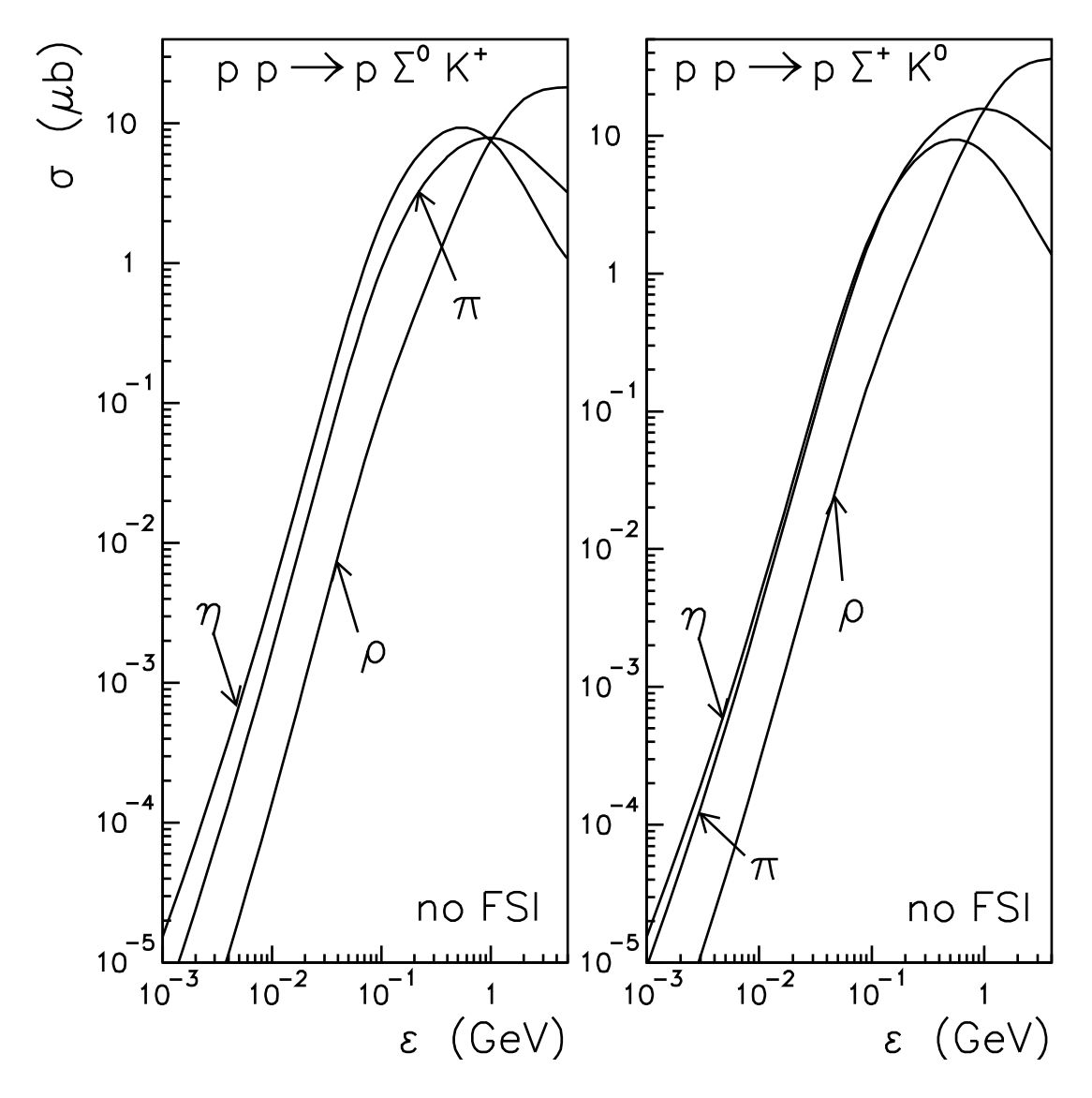


Figure 3: Decomposition of the total cross section in terms of individual meson exchange contributions, π , η and ρ -meson exchanges for the $pp \rightarrow p\Sigma^0 K^+$ and $pp \rightarrow p\Sigma^+ K^0$ reactions using $g_{\eta NN} = 7.9$.

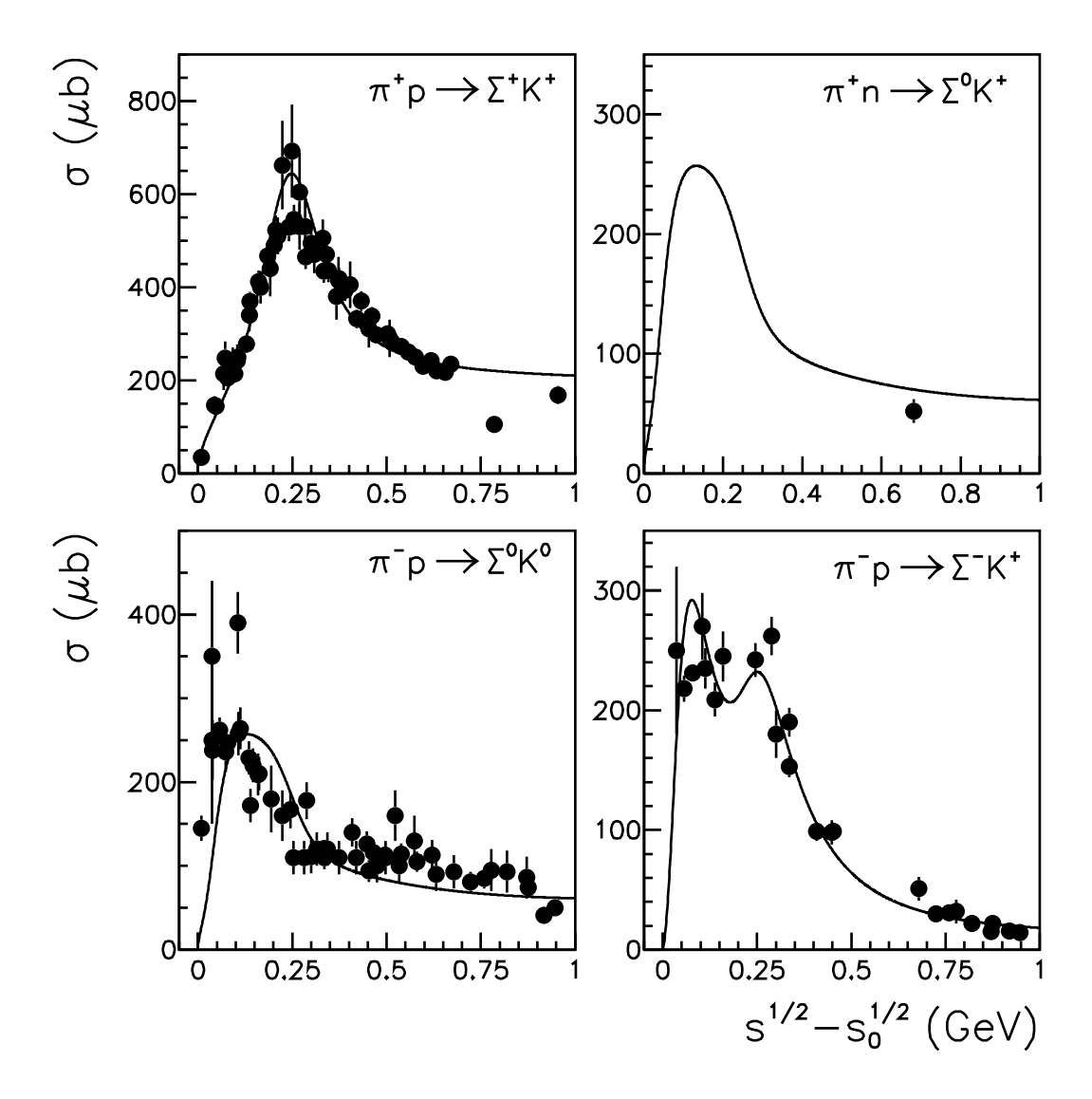


Figure 4: Energy dependence of the total cross sections for the $\pi^+ p \rightarrow K^+ \Sigma^+$, $\pi^- p \rightarrow K^0 \Sigma^0$, $\pi^+ n \rightarrow K^+ \Sigma^0$ and $\pi^- p \rightarrow K^+ \Sigma^-$ reactions as a function of the excess energy above the reaction threshold. The experimental data (full dots with error bars) are taken from Ref. [22] while the solid lines show our calculations.

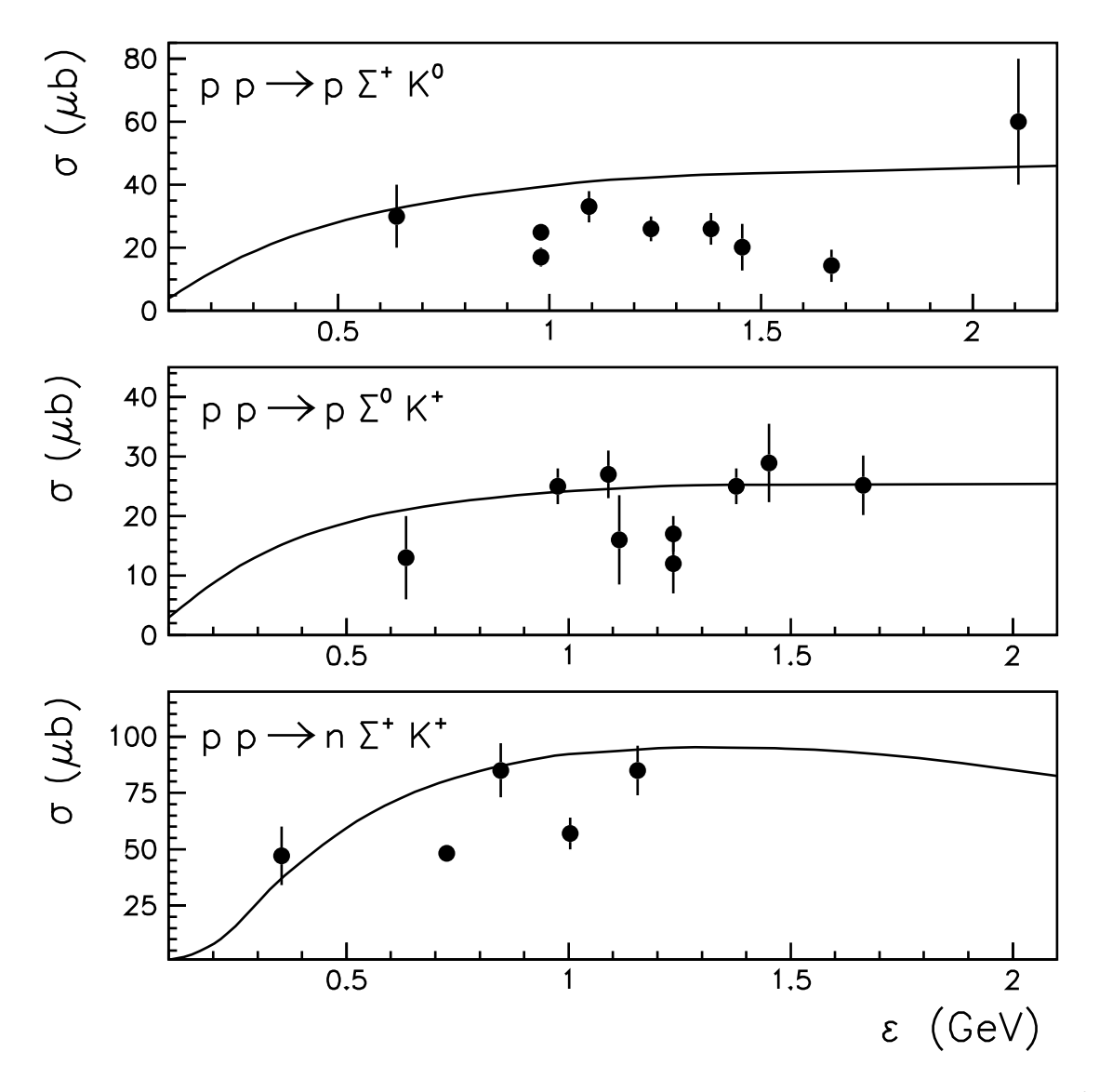


Figure 5: Energy dependence of the total cross sections for the $pp \rightarrow p\Sigma^+ K^0$, $pp \rightarrow p\Sigma^0 K^+$ and $pp \rightarrow n\Sigma^+ K^+$ reactions as a function of the excess energy ϵ above the reaction threshold. The experimental data (full dots with error bars) are taken from Ref. [22] while the solid lines show the calculations performed without the inclusion of final state interactions.

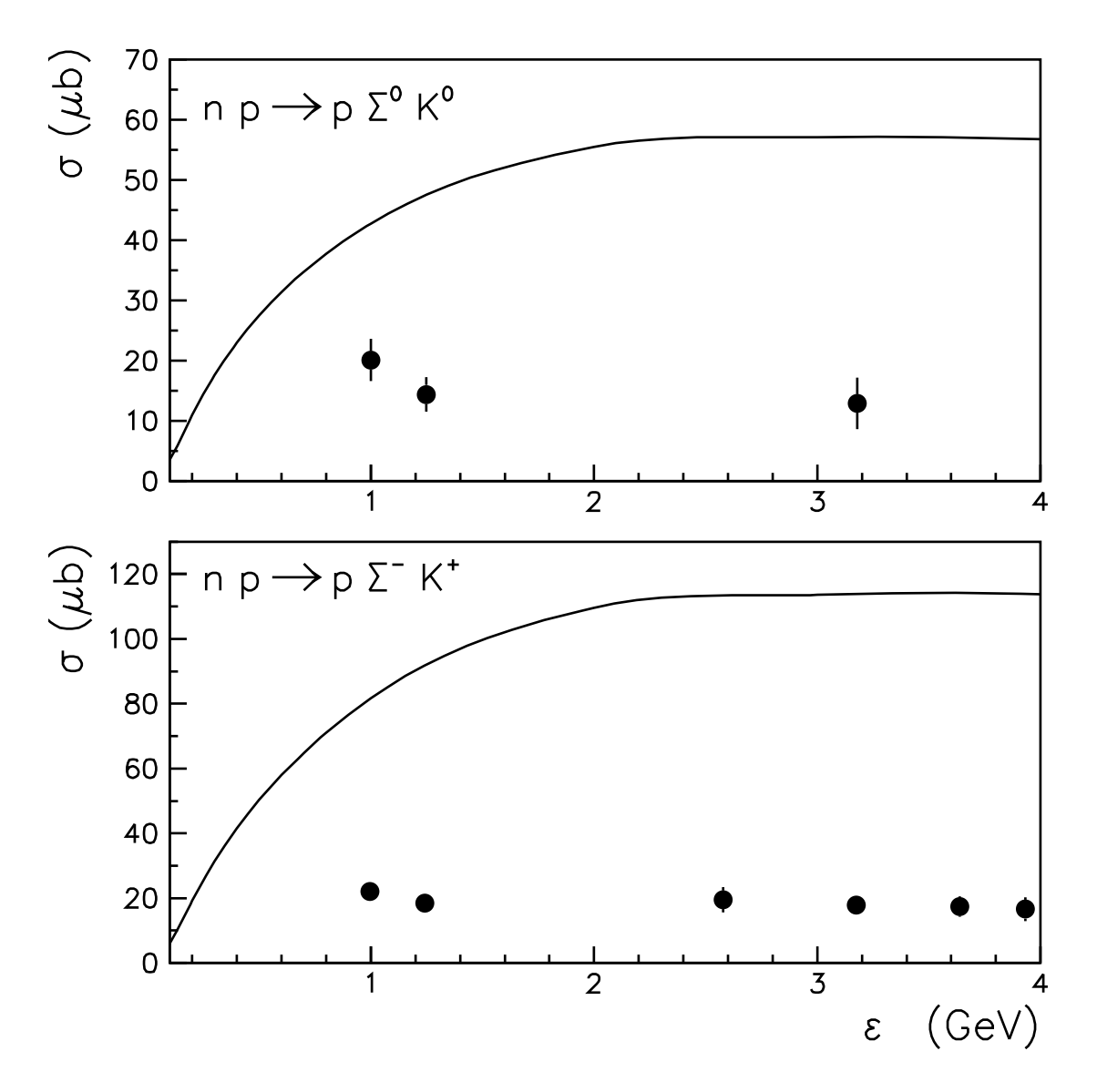


Figure 6: Energy dependence of the total cross sections for the $np \rightarrow p\Sigma^0 K^0$ and $np \rightarrow p\Sigma^- K^+$ reactions; same notation as in Fig. 5.

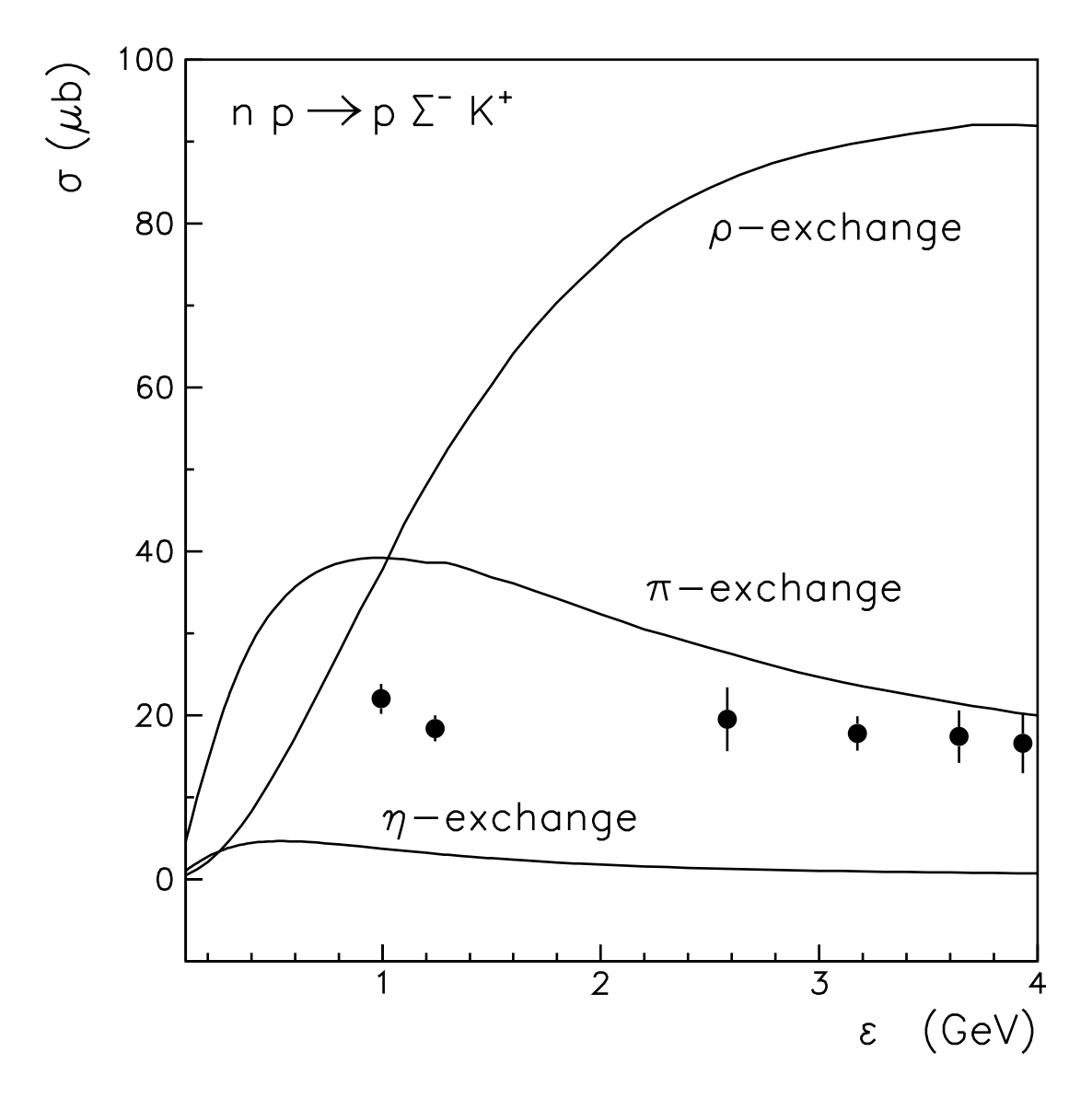


Figure 7: Decomposition of the total cross section in terms of meson exchange contributions, π , η and ρ -meson exchanges, for the $np \rightarrow p\Sigma^-K^+$ reaction.

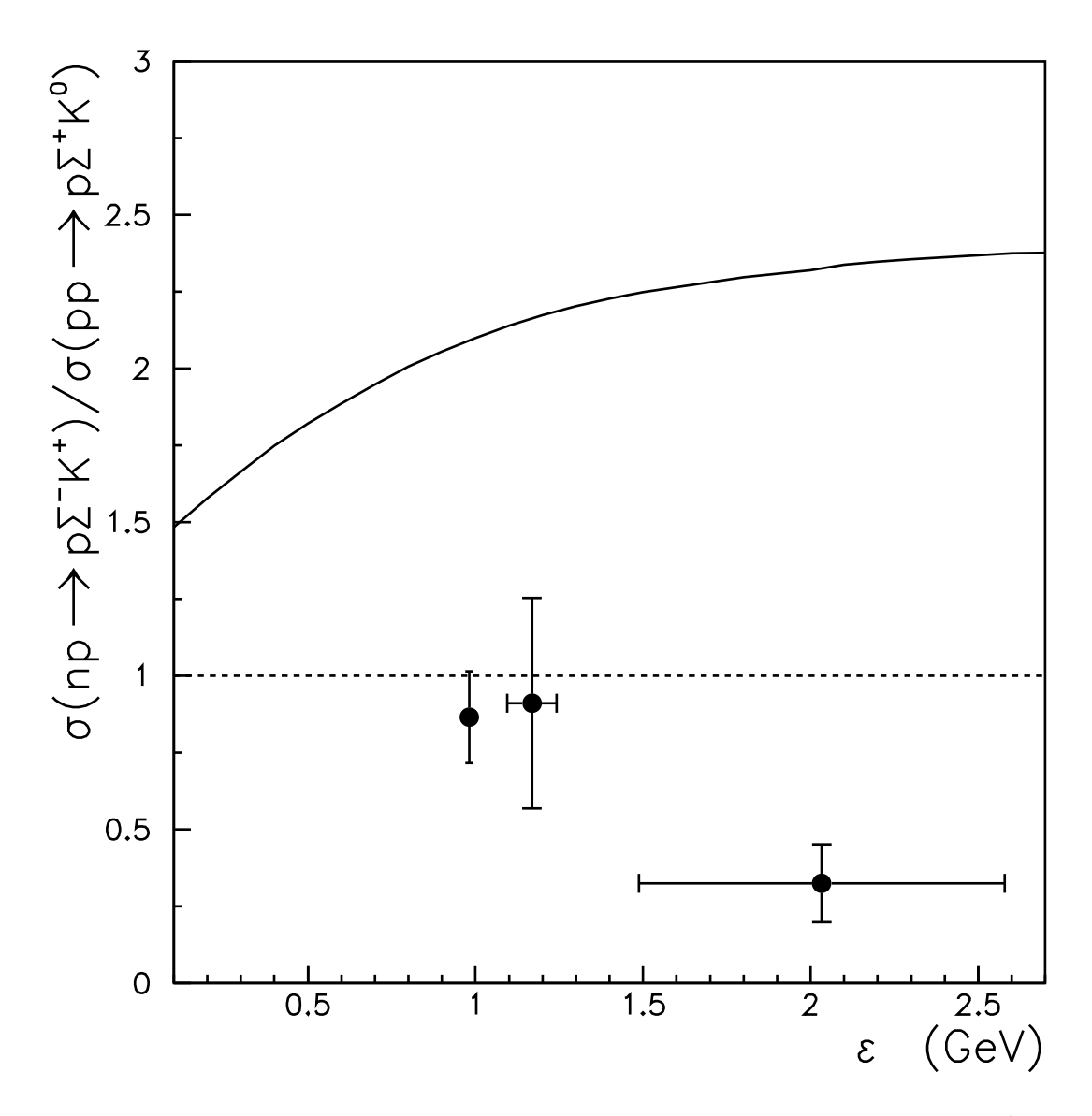


Figure 8: Ratios of the $np \rightarrow p\Sigma^-K^+$ total cross section to that for $pp \rightarrow p\Sigma^+K^0$. The ratios for the experimental data (full dots with error bars) are taken from Ref. [22], while the solid line shows the ratio for the calculated results.

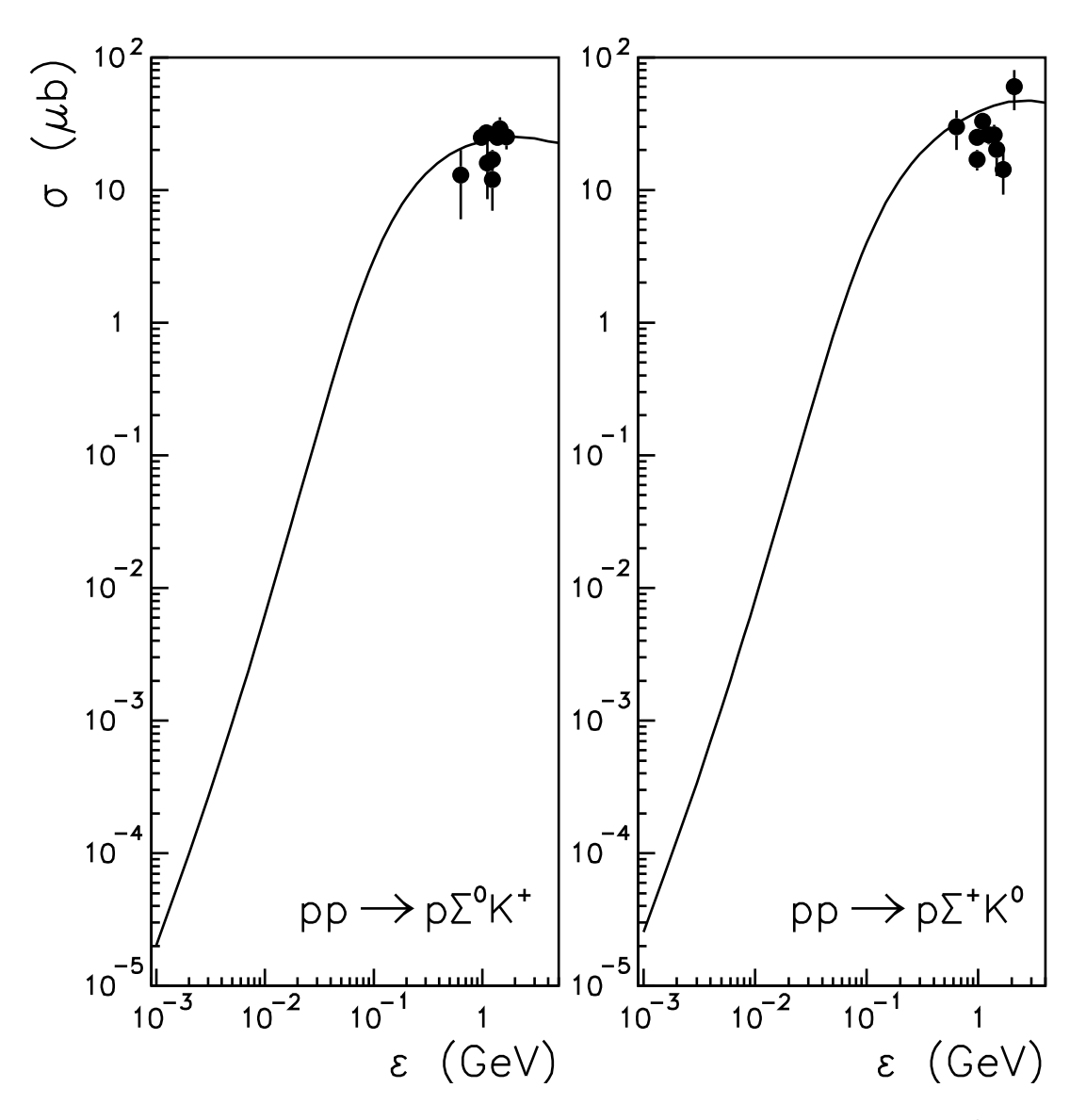


Figure 9: Energy dependence of the total cross sections for the $pp \rightarrow p\Sigma^0 K^+$ and $pp \rightarrow p\Sigma^+ K^0$ reactions as a function of the excess energy ϵ above the reaction threshold. Note that the final state interaction is not included; it is expected to be important at energies very close to the threshold.

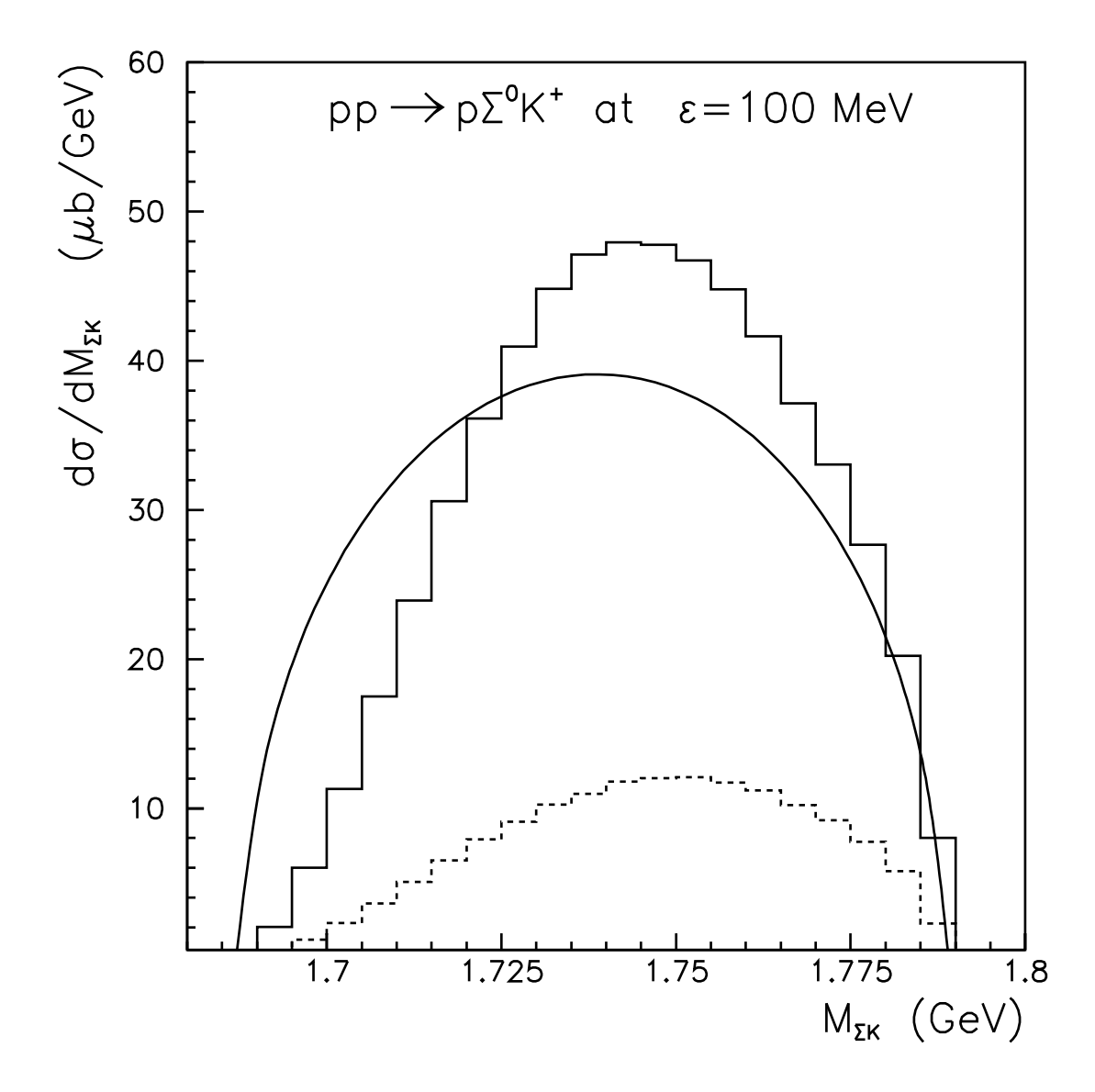


Figure 10: Calculated invariant mass distribution for the ΣK system produced in the $pp{\to}p\Sigma^0K^+$ reaction at an excess energy of 100 MeV. The dashed histogram shows the sum of the contribution from the N(1720) and $\Delta(1920)$ resonances, while the solid histogram shows the total contribution from the N(1710), N(1720) and $\Delta(1920)$ resonances. The solid line is a phase-space distribution normalized to the same total cross section.

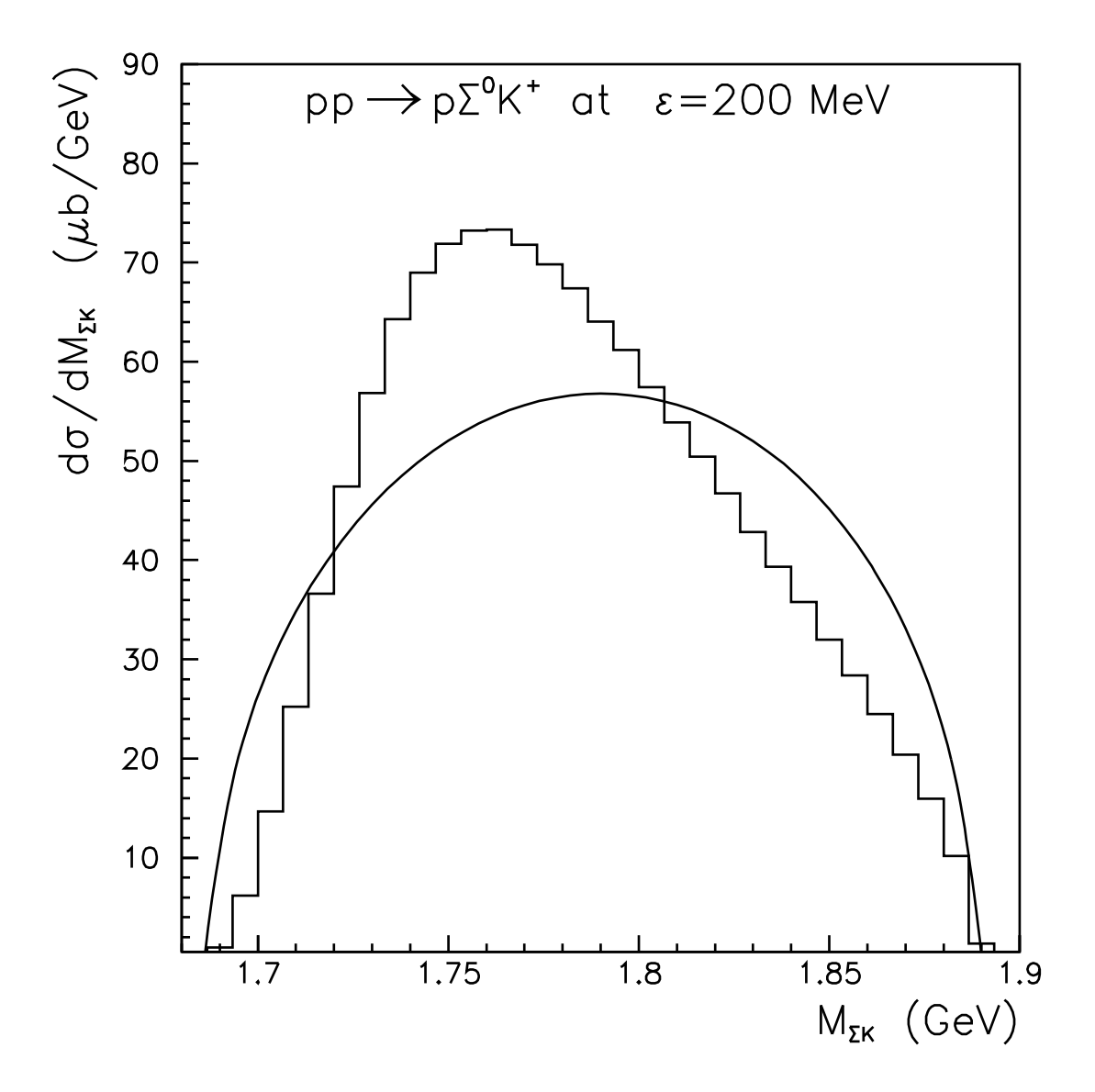


Figure 11: Same as Fig. 10 at an excess energy of 200 MeV.

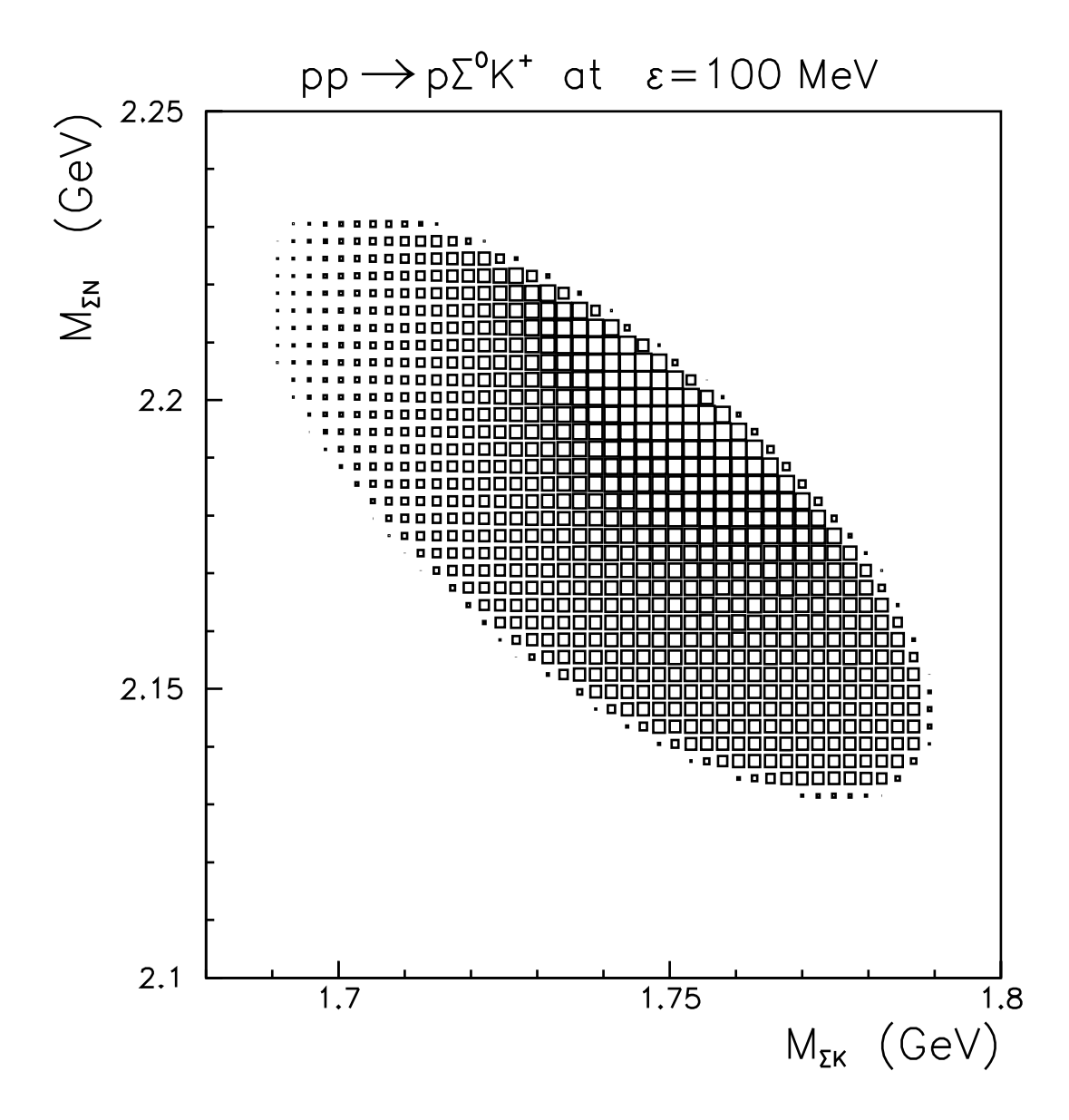


Figure 12: Dalitz plot for the $pp \rightarrow p\Sigma^0 K^+$ reaction versus $M_{\Sigma N}$ and $M_{\Sigma K}$ at an excess energy of 100 MeV. The larger squares stand for a higher density.

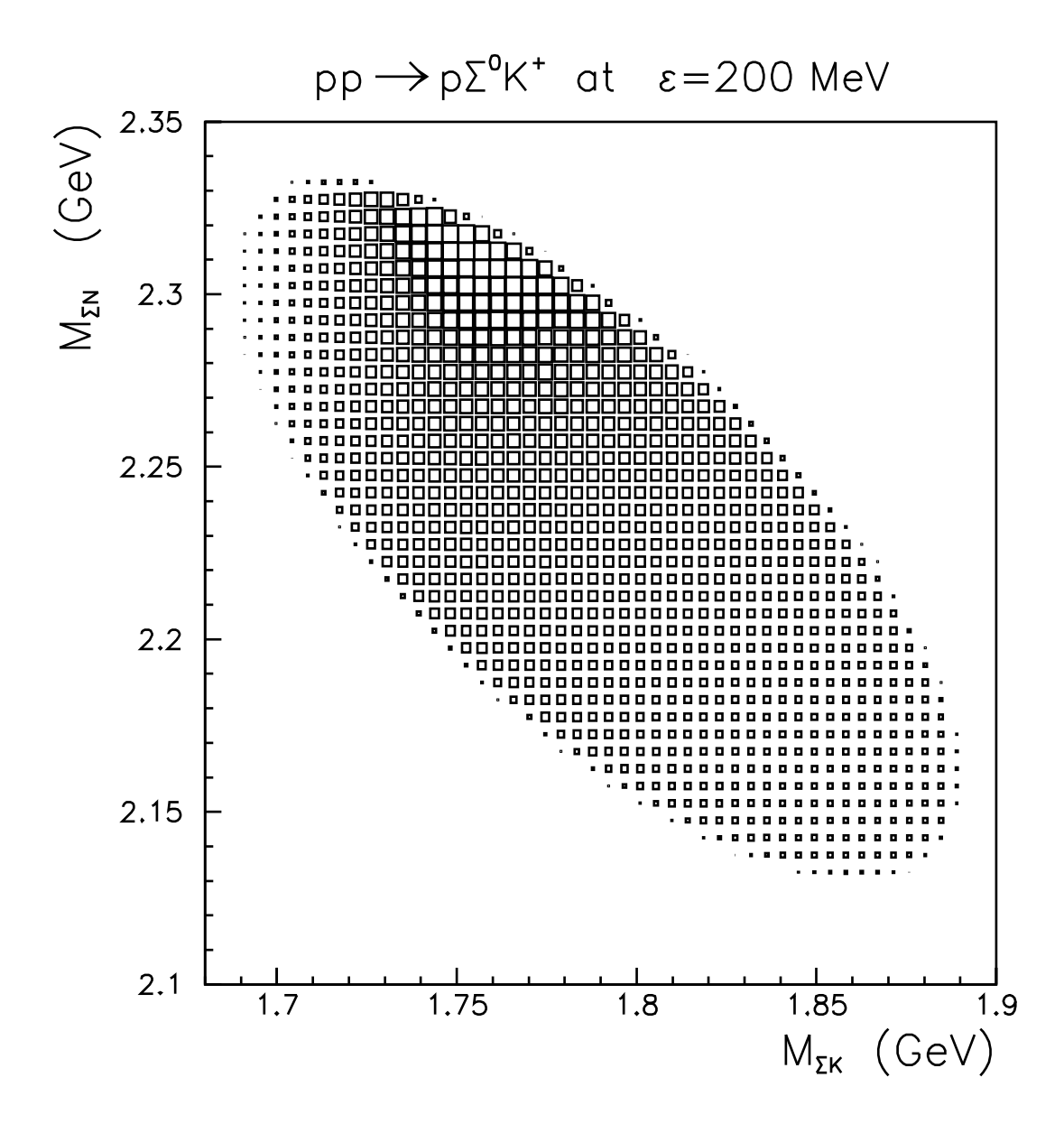


Figure 13: Same as Fig. 12 at an excess energy of 200 MeV.